2020 IEEE International Conference on Robotics and Automation (ICRA)
31 May - 31 August, 2020. Paris, France

Bidirectional Resonant Propulsion and Localization for AUVs

Thomas W. Secord[1] and Troy R. Louwagie[2]

Abstract— **Battery life, reliability, and localization are prominent challenges in the design of autonomous underwater vehicles (AUVs). This work aims to address facets of these challenges using a single system. We describe the design of a bidirectional resonant pump that uses a single electromagnetic voice coil motor (VCM) capable of rotation around a central two degree-of-freedom flexure stage axis. This actuator design produces highly efficient resonant motion that drives two orthogonally oriented diaphragms simultaneously. The operation of this diaphragm pump mechanism produces both adjustable thrust vectors at the aft surface of the AUV and a monotonic relationship between thrust vectors and operating frequency. We propose using the unique frequency to thrust relationship to enhance AUV localization capabilities. We construct a prototype and use it to experimentally demonstrate the feasibility of the directionally-tunable resonance concept.**

I. Introduction

Unmanned Underwater Vehicles (UUVs) are widely used in exploration, search and rescue, structural monitoring, and military applications. Among the different types of UUVs, remotely operated vehicles (ROVs) are most commonly employed, yet they are hindered both in cost and performance by the length and bulk of their tether to a surface ship [1]. By contrast, autonomous underwater vehicles (AUVs) hold the promise of lower operational cost and greater underwater flexibility by eliminating the need for human teleoperation through a physical tether. AUV design presents its own host of challenges. Three of the major challenges in the design and application of AUVs include power endurance, localization, and reliability.

Power endurance of AUVs is fundamentally limited based on the nearly exclusive use of propeller-based propulsion schemes. Typical electromechanical system efficiency is approximately 40% and this efficiency is substantially lower for electro-hydraulic thrusters [1]. Efforts to improve these classical systems have seen some success (e.g., [2]), yet the propeller paradigm persists even in some systems that use novel actuation technologies or methods (e.g., [3]–[7]). Many researchers attempt to improve power endurance and enhance maneuverability of AUVs using biomimetic or bio-inspired propulsion [8]. In particular, thrust produced by cephalopod jets have been of interest [9], [10], and the undulation motion of the manta ray has also shown some promise as a propulsion strategy for AUVs [11], [12]. As in many bio-inspired or bio-mimetic approaches, controllability, reliability, and precision of these mechanisms are typically sacrificed to improve efficiency or maneuverability. Thus, AUV propulsion remains a very fertile area for design improvement and paradigm shift.

Two additional challenges in AUV development are localization and overall system reliability. The multiple facets of localization difficulty are well understood (e.g., [13]) and stem mainly from the inability to use radio transmission, broad-spectrum communications, and global positioning systems (GPS) underwater given the significant attenuation of electromagnetic radiation. Acoustic underwater signals, though commonly used, still rely upon a digital paradigm (e.g., acoustic modems) for communicating positional knowledge between robots within a multi-agent arrangement [13]. Beyond assuring reliable localization, overall system reliability in AUVs is a known challenge [14], [15]. For example, Xu, Li, and Liu acknowledge that system complexity can substantially degrade reliability and they employ a fault tree technique to identify ways to improve AUV reliability. The simulated variables include AUV propulsion system leaks, steering motor faults, and propeller failures [14]. Brito and Griffiths provide an even more comprehensive catalog of actual AUV reliability issues that include propulsion motor bearing degradation, cables entangled in propellers, reduced navigation accuracy, and failures in acoustic Doppler current profilers (ADCPs) [15]. As in AUV propulsion, AUV localization and overall system reliability offer prominent avenues for improvement.

The approach described in this work attempts to address all three of the foregoing challenges within a single system. We propose a design for a single electromagnetic voice coil motor (VCM) that pivots around a central two degree-of-freedom flexure stage axis. The flexure stage is comprised of multiple flexure springs that are cut from a solid piece of material so as to allow for motion in two directions. By rotating around the central axis of the stage, the VCM produces resonant motion in two orthogonally oriented diaphragm pumps. These pumps produce adjustable thrust vectors at the aft surface of the AUV. In this paper, we amalgamate concepts drawn from prior work by combining the idea of resonance-based propulsion [16] with our previous development of resonance-based pumps [17]. We also take inspiration from novel jet-based propulsion mechanisms such as [18] and recent diaphragm propulsion ideas described in [19].

Our design addresses propulsion efficiency by using a tunable resonant frequency that is achieved through anisotropic flexure stage stiffness. The device is operated at resonance in all of its possible excitation orientations and thereby

*This work was not supported by any organization.

[1]Thomas W. Secord is an Assistant Professor of Mechanical Engineering, University of St. Thomas, 2115 Summit Ave., St. Paul, MN 55105, thomas.secord@stthomas.edu

[2]Troy R. Louwagie is a Research Assistant in the Department of Mechanical Engineering, University of St. Thomas, 2115 Summit Ave., St. Paul, MN 55105, louw1728@stthomas.edu

minimizes current input into the VCM regardless of the thrust generated at the output of the diaphragm pump mechanism. Our design also enhances AUV localization capability through a monotonic relationship between operating frequency and the thrust vector profile. When acoustically coupled to the exterior surface of the AUV, the instantaneous resonant frequency of pump operation directly broadcasts the AUV's thrust vectors to neighboring AUVs or stationary acoustic receivers. This technique avoids the standard digital communication paradigm and encodes what would normally be multiple bytes of thrust information into a single frequency. Finally, our proposed design achieves high reliability in multiple ways: 1) reduced part count compared to standard propeller designs; 2) mechanical component isolation using actuated diaphragms; 3) a high cycle flexure-based linear bearing mechanism; and 4) standard off-the-shelf actuators and components.

II. AUV Design Concept

Fig. 1 (a) shows the design of an AUV that utilizes resonant pumps to apply forward thrust as well as pitch and yaw moments using thrust vectors at the aft surface of the AUV. The two resonant pumps are oriented at right angles within the AUV housing as shown in Fig. 1 (b). In this concept, one pump controls the yaw, one pump controls the pitch, and both pumps contribute to forward thrust applied to the AUV. Each pump drives the motion of two diaphragms based on the orientation of a single voice coil motor (VCM) around the central axis of a two degree-of-freedom flexure stage. The diaphragm motions provide positive displacement pumping through two sets of diametrically opposed channels that span the length of the AUV and terminate in check valves.

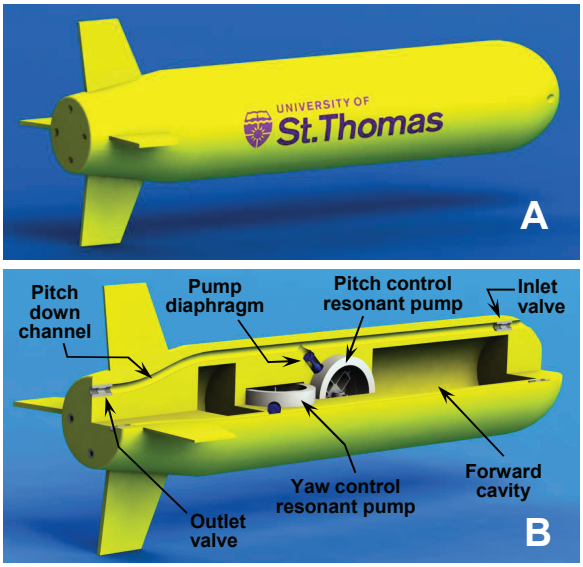

Fig. 1. AUV design concept. (a) Fully assembled AUV. (b) Cross sectional view of the AUV showing the pitch and yaw resonant pump thrust mechanisms.

In order to change the flow through each channel, and thereby maneuver the AUV, the orientation of the pitch or yaw pump VCM is adjusted using rotation of a carriage ring to which the VCM is attached. This rotational change is only required intermittently and can be provided by a standard DC gear-motor. As the VCM orientation is changed, the displacement of each diaphragm (and therefore the stroke volume) varies according to the displacement of the flexure stage. Like magnetically coupled actuators (such as in [3]), our pump design isolates the mechanism components from the fluid environment. The operating principle of the mechanism is described in more detail below.

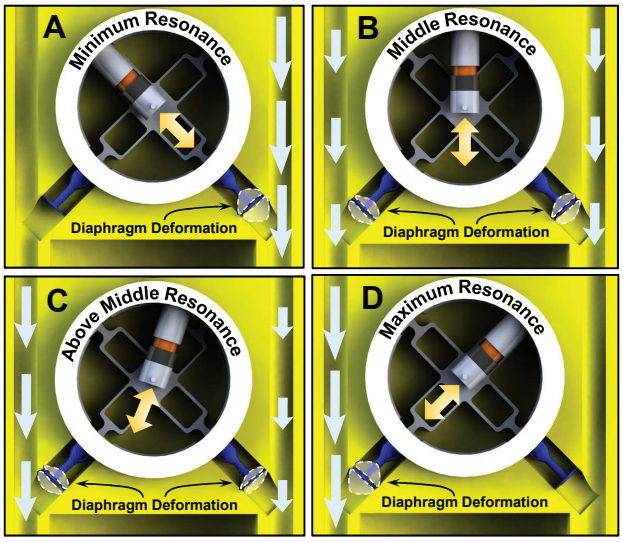

Fig. 2. Operating principle of the resonant pump system using a radially directed VCM. (a) Minimum resonant frequency; zero flow in the left channel (b) Operation at a mid-range resonant frequency to equalize channel flow. (c) Operation near the maximum resonant frequency to favor flow in the left channel. (d) Operation at maximum resonance; zero flow in the right channel.

Fig. 2 shows the operating principle of the pump system. The most salient feature of this design is that the two-degree of freedom flexure stage exhibits different resonant frequencies based on the orientation of the excitation force from the radially directed VCM. We explore this idea quantitatively in Section III-A. Flexure stages commonly exhibit resonant frequencies, yet they are considered undesirable behaviors from a position control perspective [20]. In our design, we operate in an open-loop fashion and deliberately excite the fundamental resonant frequency of the flexure stage at the given orientation of the VCM. In this way, resonance is used advantageously to minimize the power required to drive the voice coil. Others have also shown viability of the resonance approach in underwater propulsion [16], [21]–[23]. Hence, the present approach holds significant promise for enhancing AUV power endurance and longevity through increased propulsion efficiency.

In Fig. 2 (a), the flexure and diaphragm system is shown at resonance in the most compliant direction. The associated flow is maximum in the right channel causing the most

aggressive directional change. For example, in the pitch control usage, this resonant frequency would yield the most aggressive possible pitch maneuver in the associated direction of the AUV pitch. Fig. 2 (b) and (c) show the resonance of the flexure stage and diaphragm in between the two resonance extremes. By moving between the two resonance extremes, flow is modulated between the channels as dictated by the stroke volume and frequency of the particular resonant pump design. Hence, moving between resonance extremes will causing more gradual veering motion in pitch or yaw. Finally, Fig. 2 (d) shows the resonance of the flexure stage and diaphragm in the stiffest direction. The associated flow is maximum in the left channel causing the most aggressive turning moment about the associated pitch or yaw axis.

III. Dynamics of Resonant Propulsion

We begin by considering the dynamics of resonance-based propulsion pumps using a simplified model for a single pump mechanism. We then discuss the considerations for diaphragm design to ensure that the desired flow rates are achieved despite different frequencies of diaphragm motion across the range of excitation angles illustrated in Fig. 2.

A. Angular Dependence of Resonant Frequency

We represent the dynamics of the resonant propulsion system using the simple lumped parameter model shown in Fig. 3. The model consists of a stiffness along each axis (K_x, K_y), a viscous damping effect along each axis (D_x, D_y), a central mass (M) representing the flexure stage and any of its translating components, added mass elements (M_{ax}, M_{ay}) associated with each diaphragm-fluid interaction, and a force (F_{VCM}) from the voice coil applied at an angle with respect to the principal x- and y-axis directions.

This model is intended to undergo relatively small displacement in both the x and y directions, so we approximate the spring deformations using only the values of the displacement coordinates of x and y. In our model development we define the x direction of the pump to be the stiffer direction and therefore the direction along which the resonant frequency is the largest. We also assume that the flexure stage behaves as a single degree-of-freedom, second-order, oscillating system with only a single, dominant resonant mode, the frequency of which can be determined by the excitation angle of the VCM with respect to the x and y directions. Lastly, we assume that the AUV accelerations are small and that the ground reference in Fig. 3 can be treated as an inertial frame.

If F_{VCM} is a static force, then the deformation of each diaphragm in the pump is given by

$$x = \frac{F_{VCM}\cos\theta}{K_x} \qquad y = \frac{F_{VCM}\sin\theta}{K_y} \tag{1}$$

We will define the net displacement of the central stage mass as $\delta \triangleq \sqrt{x^2+y^2}$ and the equivalent stiffness as $K_{eq} \triangleq F_{VCM}/\delta$. With these definitions, the equivalent stiffness becomes

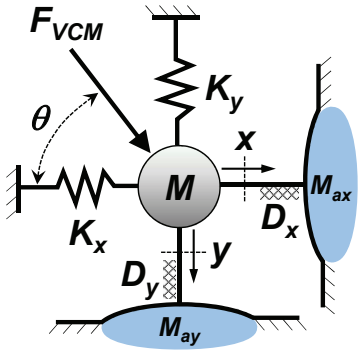

Fig. 3. Lumped parameter model of the bidirectional resonant pump system subject to voice coil motor excitation.

$$K_{eq} = K_x \frac{\gamma}{\sqrt{\gamma^2\cos^2\theta + \sin^2\theta}} \tag{2}$$

where we have used an additional definition of the dimensionless ratio between the x- and y-axis stiffness values: $\gamma \triangleq K_y/K_x$, which we take to be between 0 and 1 because the x-axis represents the stiffest direction of the stage from our previously stated assumption.

The natural frequency, $f_n(\gamma,\theta)$, of the stage is now recognized to be a function of the angle of excitation θ and the value of the stiffness ratio γ. If we assume that $M >> M_{ax}$ and $M >> M_{ay}$, then the natural frequency can be written as

$$f_n(\gamma,\theta) = \frac{1}{2\pi}\sqrt{\frac{K_x}{M}}\sqrt{\frac{\gamma}{\sqrt{\gamma^2\cos^2\theta+\sin^2\theta}}} \tag{3}$$

The assumption regarding small added mass is made only for model simplification purposes. Added mass terms can be re-inserted with an associated angular dependence should this become necessary for certain resonant pump designs. The natural frequency of the stage during pure x-axis excitation will be denoted by $\omega_{nx} = \sqrt{K_x/M}$. We shall define the second square root term of (3) to be a scalar function $\Phi(\gamma,\theta)$. Hence, (3) is now more compactly written as

$$f_n(\gamma,\theta) = \frac{1}{2\pi}\omega_{nx}\Phi(\gamma,\theta) \tag{4}$$

If we also assume that the equivalent damping, D_{eq}, for an arbitrary excitation angle θ can be written in the same form as (2), then the equivalent stiffness and damping are now written as

$$K_{eq} = K_x\Phi^2(\gamma,\theta) \qquad D_{eq} = D_x\Phi^2(\lambda,\theta) \tag{5}$$

where $\lambda \triangleq D_y/D_x$ is the ratio of the viscous damping along each axis and $\Phi(\lambda,\theta)$ is the same scalar function as $\Phi(\gamma,\theta)$ but with λ taking the place of γ.

Our primary interest is in the displacement amplitude of the central stage since this will determine the displacement of each diaphragm as represented in Fig. 2 and Fig. 3. We now take the VCM force to be of the form $F_{VCM}(t) = F_0\sin(\omega t)$.

Therefore, the DC displacement of the system is F_0/K_{eq}. In response to this sinusoidal excitation, the steady state displacement amplitude (normalized with respect to the DC displacement) can be written using the standard second-order system frequency response as

$$A(\bar{\omega},\gamma,\lambda,\theta,\zeta_x) = \frac{\Phi^2(\gamma,\theta)}{\sqrt{(\Phi^2(\gamma,\theta)-\bar{\omega}^2)^2+4\zeta_x^2\Phi^4(\lambda,\theta)\bar{\omega}^2}} \tag{6}$$

where we have introduced the x-axis vibration damping ratio using the familiar relationship $\zeta_x = D_x/\sqrt{4K_xM}$ and we have also introduced the dimensionless frequency $\bar{\omega} \triangleq \omega/\omega_{nx}$.

To illustrate the use of this equation, we selected $\lambda = 1$, $\gamma = 0.5$, and $\zeta_x = 0.1$. The resulting frequency response amplitude contours of (6) are shown in Fig. 4. In Fig. 4, the peak displacement amplitude is normalized to a value of 1 for excitation along the x-axis. For our selected values of λ, γ, and ζ_x, the frequency response magnitude function exhibits a strong resonant peak at the various excitation angles between 0° and 90°. The frequency at which peak displacement occurs shifts downward as the excitation angle is increased. This downward shift is the result of the downward shift in K_{eq}. Hence, for highly efficient operation of the pump-based thruster system, the excitation frequency for a given excitation angle must reside in the red (i.e. highest) contour of Fig. 4. In the case of planar AUV maneuvering, the unique resonant frequency for each angle of stage excitation has the added benefit of providing a monotonic relationship between pump operating frequency and the forces and moments applied to the AUV. This allows for enhanced multi-robot localization as discussed in Section IV.

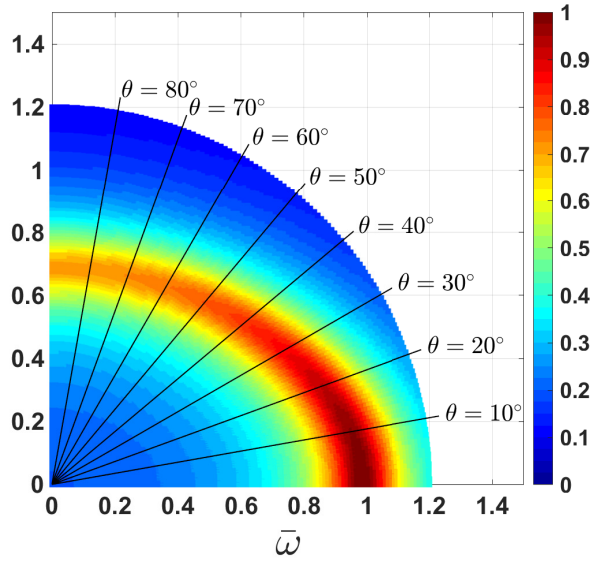

Fig. 4. Contours of normalized displacement amplitude versus normalized excitation frequency for the bidirectional resonant device.

To further illustrate the monotonicity of the relationship between resonant frequency (i.e., optimal pump operating frequency) and excitation angle θ, Fig. 5 shows the frequency response of the flexure stage at three angles: 0°, 45°, and 90°. These frequency response curves represent radial slices of Fig. 4 along the corresponding θ line. For the plot in Fig. 5, we have selected $\gamma = 0.75$, $\lambda = 0.9$, and $\zeta_x = 0.1$. For these design parameter values, the frequency response peak amplitude remains relatively constant and the 45° excitation direction yields a resonant frequency that is approximately midway between the 0° and 90° extremes. As shown in Section V, behavior consistent with these model parameters can be realized in practice.

B. Diaphragm Design

We will assume that thrust vectors T_x and T_y arise from the jets of water exiting the diametrically opposed aft valves and that these thrusts are proportional to the corresponding volumetric flow rates Q_x and Q_y in the x and y channels, respectively. Letting this proportionality constant be denoted by τ, we have

$$T_x = \tau Q_x \qquad T_y = \tau Q_y \tag{7}$$

Though more elaborate thrust models are possible (e.g., [24]), the flow rate from the x-axis side of the diaphragm pump will be approximately

$$Q_x = \left(\frac{\alpha_x F_0 \omega \cos\theta}{2\pi K_x \Phi^2(\gamma,\theta)}\right) A(\bar{\omega},\gamma,\lambda,\theta,\zeta_x) \tag{8}$$

where α_x is the equivalent area of the diaphragm such that the product of this area and the stroke yields the stroke volume for the diaphragm associated with the x-axis. All other parameters remain as previously defined. A similar area, α_y, and flow rate Q_y are defined for the orthogonal y-axis diaphragm.

A logical design goal is to achieve thrust out of a single channel that is equal when the VCM is oriented at 0° and 90°. To achieve this, we combine (7) and (8) to define the required ratio for the diaphragm effective areas:

$$\frac{\alpha_x}{\alpha_y} = \frac{A(\sqrt{\gamma},\gamma,\lambda,90°,\zeta_x)}{\gamma A(1,\gamma,\lambda,0°,\zeta_x)} \tag{9}$$

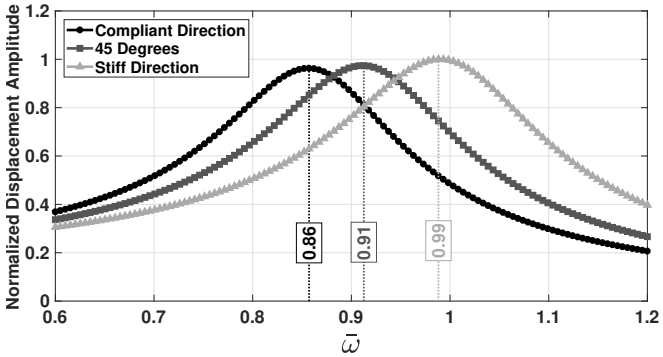

Fig. 5. Displacement amplitude response versus normalized frequency for the bidirectional resonant device in the most compliant, middle, and least compliant directions.

In (9), the amplitude response function has been evaluated at $\bar{\omega} = 1$ for the x-axis excitation (0°) while it has been evaluated at $\bar{\omega} = \sqrt{\gamma}$ for the y-axis excitation (90°) since $\bar{\omega}_{ny} = \omega_{ny}/\omega_{nx} = \sqrt{\gamma}$. If the diaphragms are designed to satisfy (9), then equal thrust is expected at the two extremes of θ.

IV. Acoustic Localization

As discussed in Section III-A, for an AUV operating in only pitch (up-down) or yaw (left-right) maneuvers, there is a monotonic relationship between the frequency of the pump and the specific thrust vector profile generated at the aft valves. This implies that the acoustic emission from a resonant pump can be used to broadcast an individual AUV's thrust setting to neighboring AUVs. In this concept, we assume that the AUV is sufficiently close to neighboring AUVs such that the actuators need only resonate at relatively low underwater acoustic transmission frequencies (i.e., $\approx$ 10 Hz - 300Hz [25]). This technique avoids the standard digital communication paradigm and instead encodes multiple bytes of thrust information into a single frequency. This general concept is shown in Fig. 6.

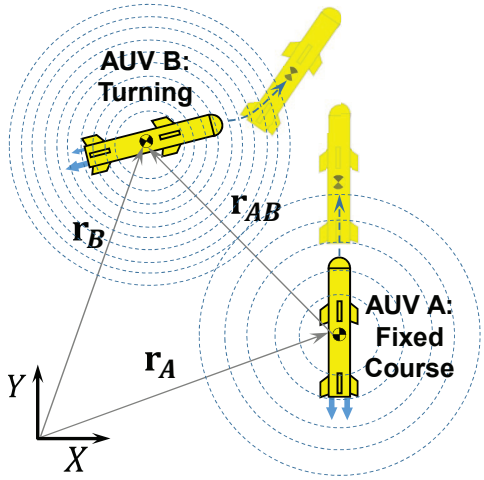

Fig. 6. Acoustic localization principle for monotonic frequency to thrust relationships of the AUVs.

Fig. 6 shows AUV B performing an aggressive left turn, which would require a high frequency excitation of the resonant pump's flexure stage along a direction close to $\theta = 0°$. At this frequency, the pump provides a preferential thrust in AUV B's right flow channel per Fig. 2. This high frequency acoustic transduction is detected by AUV A and used in conjunction with its own internal position estimate $\hat{\mathbf{r}}_A$ to update $\hat{\mathbf{r}}_B$ and thereby update $\hat{\mathbf{r}}_{AB} = \hat{\mathbf{r}}_B - \hat{\mathbf{r}}_A$.

Once a neighboring AUVs thrust profile is known at a given instant (e.g., from hydrophone data), this thrust can be used in an online observer. For example, the Extended Kalman Filter (EKF) commonly used in land based simultaneous localization and mapping (SLAM) can be viable in this situation [26]. The EKF would continually update the various position vectors $\mathbf{r}_A$, $\mathbf{r}_B$, and $\mathbf{r}_{AB}$ shown in Fig. 6. Though thrust vector information would be insufficient for accurate localization on its own, it would provide a useful contribution to sensor fusion approaches. In short, multi-agent or cooperative localization techniques described in [27] can be applied to good effect provided that the challenges unique to underwater communication (e.g., surface reflections) are accounted for in the algorithm [13], [28]. Our future work will explore how strongly the acoustic emission of the pump-based system can be transmitted into surrounding fluid medium in order to determine the effective range of our proposed technique.

V. Experimental Prototype

Fig. 7 shows the experimental prototype for the bidirectional resonant flexure stage system. In this initial prototype, we have not coupled the stage axes to diaphragms pumps, yet all other essential features such as directional stiffness dependence, VCM excitation, and rotating carriage ring are all included. We employ a flexure stage kinematic structure described in [20] with a modification to reduce stiffness by using only single flexure columns in the x and y directions. In future pump versions, all of the well established flexure design techniques for two degree-of-freedom stages (e.g., [29], [30]) can be employed to further enhance axis decoupling and minimize parasitic rotations.

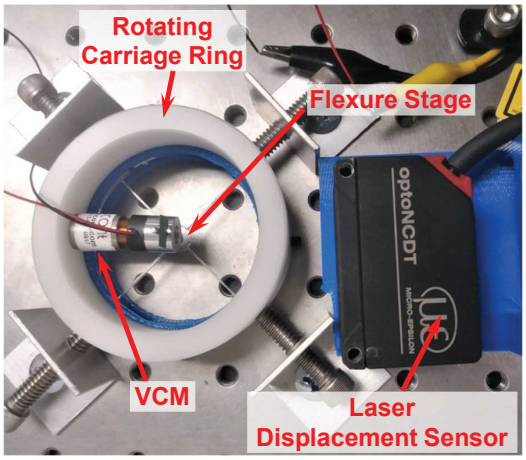

Fig. 7. Experimental test setup for the bidirectional oscillator prototype.

The detailed schematic of our test setup is provided in Fig. 8. We drive the voice coil motor (Moticont LVCM-010-013-01) using a linear power amplifier (Gain = 2) whose input is obtained from a function generator (Agilent 33120A) set to provide a 200 mV peak-to-peak sinusoidal voltage sweep from 10 Hz to 80 Hz in a linearly spaced span of 20 seconds. Both the current and voltage in the voice coil are measured by a National Instruments NI6215 USB-based data acquisition card set to sample at at 500 Hz. The displacement along the direction of excitation is measured using a laser displacement sensor (Micro-Epsilon optoNCDT 1420-25). All signals are stored using LabVIEW running on a data acquisition desktop computer.

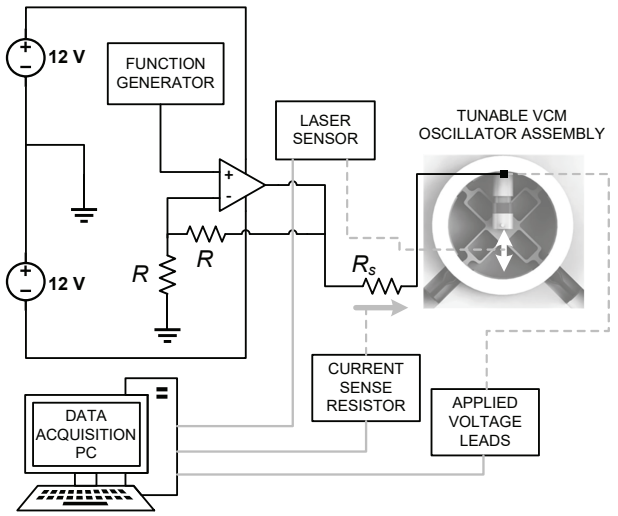

Fig. 8. Schematic of the experimental setup for the bidirectional oscillator prototype.

Using the setup described above, we collected resonance data at three different directions of excitation: 1) along the most compliant direction (i.e., *y*-axis); 2) along the stiffest direction (i.e., *x*-axis); and 3) midway between these two extremes at an angle of 45°. At each orientation we computed the ratio of FFTs between input current signal (A) and output displacement signal (mm). The results shown in Fig. 9 exhibit the dynamic behavior described in Section III-A and model output in Fig. 5. Moreover, the experimental results incorporate a crucial aspect of efficiency: current input into the actuator. The plotted metric in Fig. 9 illustrates the benefit of resonance wherein at least a three-fold increase in the displacement per unit of current is obtained relative to DC or above-resonance operation. This is in stark contrast to the typical UUV propulsion paradigm where continuously rotating propeller mechanisms provide no resonance benefit.

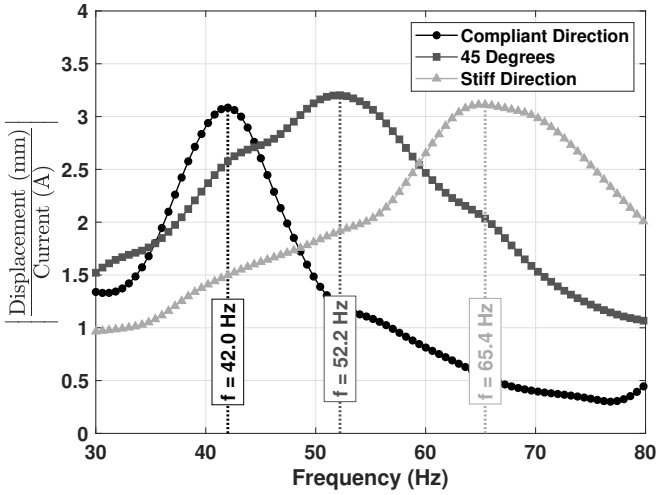

Fig. 9. Resonance data collected from a simplified resonant propulsion prototype.

VI. Conclusions and Future Work

We have described a bidirectional resonance-based diaphragm pumping mechanism that can be used to propel AUVs using a small number of readily fabricated components. In addition to operating efficiently at resonance, the device operating frequency can encode the thrust vector configuration of the AUV so that neighboring AUVs can better estimate relative and absolute positions. Our design minimizes the component count and surface interfaces associated with rotary and linear bearings by using a flexure based suspension and deforming diaphragms. Reduced component count and flexure-based mechanisms are expected to increase AUV propulsion system reliability. Our future work will focus on implementing and testing specific diaphragm designs for optimal thrust generation at the scale of typical AUVs. The performance of the localization system may also exhibit depth dependence and issues attendant with traditional acoustic sensing, which we also plan to assess in future work.

Given the monotonic relationship between thrust vectors and operating frequency, useful information is encoded in the operating frequency of the pumps themselves. In its current conceptual form, the localization principle described in Section IV requires only simple hydrophone sensors. If we assume the AUV has identical pitch and yaw pump mechanisms, our approach would be limited to scenarios in which multiple AUVs are performing maneuvers in one plane of motion (e.g. pitching up or down; turning left or right) at a time so as to avoid confounding between frequencies producing pitch motions or frequencies producing yaw motions. However, this limitation can be overcome by designing the yaw and pitch pumps to operate within non-overlapping frequency ranges. Such designs form the basis for ongoing and future work. Overall, the bidirectional resonant pump mechanism addresses multiple challenges within AUV design and provides a promising foundation for further development.

References

[1] L. L. Whitcomb, "Underwater robotics: Out of the research laboratory and into the field," in *Proceedings 2000 ICRA. Millennium Conference. IEEE International Conference on Robotics and Automation. Symposia Proceedings (Cat. No. 00CH37065)*, vol. 1. IEEE, 2000, pp. 709–716.

[2] B. Allen, W. S. Vorus, and T. Prestero, "Propulsion system performance enhancements on REMUS AUVs," in *OCEANS 2000 MTS/IEEE Conference and Exhibition. Conference Proceedings (Cat. No. 00CH37158)*, vol. 3. IEEE, 2000, pp. 1869–1873.

[3] E. P. Vega, O. Chocron, and M. Benbouzid, "A flat design and a validated model for an AUV reconfigurable magnetic coupling thruster," *IEEE/ASME Transactions on Mechatronics*, vol. 21, no. 6, pp. 2892–2901, 2016.

[4] X. Li, D. Chen, J. Jin, and L. Wang, "A novel underwater piezoelectric thruster with one single resonance mode," *Review of Scientific Instruments*, vol. 90, no. 4, p. 045007, 2019.

[5] E. Cavallo, R. C. Michelini, and V. F. Filaretov, "Conceptual design of an AUV equipped with a three degrees of freedom vectored thruster," *Journal of Intelligent and Robotic Systems*, vol. 39, no. 4, pp. 365–391, 2004.

[6] L. Pugi, B. Allotta, and M. Pagliai, "Redundant and reconfigurable propulsion systems to improve motion capability of underwater vehicles," *Ocean Engineering*, vol. 148, pp. 376–385, 2018.

[7] S. A. Watson and P. N. Green, "Propulsion systems for micro-autonomous underwater vehicles (μAUVs)," in *2010 IEEE Conference on Robotics, Automation and Mechatronics*. IEEE, 2010, pp. 435–440.

[8] M. Mojarrad, "AUV biomimetic propulsion," in *OCEANS 2000 MTS/IEEE Conference and Exhibition. Conference Proceedings (Cat. No. 00CH37158)*, vol. 3. IEEE, 2000, pp. 2141–2146.

[9] K. Mohseni, "Pulsatile vortex generators for low-speed maneuvering of small underwater vehicles," *Ocean Engineering*, vol. 33, no. 16, pp. 2209–2223, 2006.

[10] F. Giorgio-Serchi, A. Arienti, and C. Laschi, "Underwater soft-bodied pulsed-jet thrusters: Actuator modeling and performance profiling," *The International Journal of Robotics Research*, vol. 35, no. 11, pp. 1308–1329, 2016.

[11] C.-M. Chew, Q.-Y. Lim, and K. Yeo, "Development of propulsion mechanism for robot manta ray," in *2015 IEEE International Conference on Robotics and Biomimetics (ROBIO)*. IEEE, 2015, pp. 1918–1923.

[12] K. W. Moored, P. A. Dewey, M. C. Leftwich, H. Bart-Smith, and A. J. Smits, "Bioinspired propulsion mechanisms based on manta ray locomotion," *Marine Technology Society Journal*, vol. 45, no. 4, pp. 110–118, 2011.

[13] L. Paull, S. Saeedi, M. Seto, and H. Li, "AUV navigation and localization: A review," *IEEE Journal of Oceanic Engineering*, vol. 39, no. 1, pp. 131–149, 2013.

[14] H. Xu, G. Li, and J. Liu, "Reliability analysis of an autonomous underwater vehicle using fault tree," in *2013 IEEE International Conference on Information and Automation (ICIA)*. IEEE, 2013, pp. 1165–1170.

[15] M. P. Brito and G. Griffiths, "A markov chain state transition approach to establishing critical phases for AUV reliability," *IEEE Journal of Oceanic Engineering*, vol. 36, no. 1, pp. 139–149, 2011.

[16] T. W. Secord, A. Mazumdar, and H. H. Asada, "A multi-cell piezoelectric device for tunable resonance actuation and energy harvesting," in *2010 IEEE International Conference on Robotics and Automation*. IEEE, 2010, pp. 2169–2176.

[17] T. Secord and M. Audi, "A high efficiency tunable resonance pump for biomedical applications," in *2018 Design of Medical Devices Conference*. American Society of Mechanical Engineers Digital Collection, 2018.

[18] A. Mazumdar, M. S. Triantafyllou, and H. H. Asada, "Dynamic analysis and design of spheroidal underwater robots for precision multidirectional maneuvering," *IEEE/ASME Transactions on Mechatronics*, vol. 20, no. 6, pp. 2890–2902, 2015.

[19] K. Choi, "Device having a vibration based propulsion system," May 2 2017, US Patent 9,638,177.

[20] Y. K. Yong, S. S. Aphale, and S. R. Moheimani, "Design, identification, and control of a flexure-based XY stage for fast nanoscale positioning," *IEEE Transactions on Nanotechnology*, vol. 8, no. 1, pp. 46–54, 2008.

[21] X. Deng and J. Zhang, "Voice coil actuator direct-drive resonant system," Feb. 9 2017, US Patent App. 14/969,171.

[22] K. A. Harper, M. D. Berkemeier, and S. Grace, "Modeling the dynamics of spring-driven oscillating-foil propulsion," *IEEE Journal of Oceanic Engineering*, vol. 23, no. 3, pp. 285–296, 1998.

[23] C. Niezrecki and S. Balakrishnan, "Power characterization of THUNDER actuators as underwater propulsors," in *Smart Structures and Materials 2001: Smart Structures and Integrated Systems*, vol. 4327. International Society for Optics and Photonics, 2001, pp. 88–98.

[24] E. P. Vega, O. Chocron, and M. Benbouzid, "AUV propulsion systems modeling analysis," *International Review on Modelling and Simulations*, vol. 7, no. 5, pp. 827–837, 2014.

[25] J.-N. Decarpigny, B. Hamonic, and O. B. Wilson, "The design of low frequency underwater acoustic projectors: present status and future trends," *IEEE Journal of oceanic engineering*, vol. 16, no. 1, pp. 107–122, 1991.

[26] M. Bryson and S. Sukkarieh, "Building a robust implementation of bearing-only inertial SLAM for a UAV," *Journal of Field Robotics*, vol. 24, no. 1-2, pp. 113–143, 2007.

[27] S. I. Roumeliotis and G. A. Bekey, "Distributed multirobot localization," *IEEE transactions on robotics and automation*, vol. 18, no. 5, pp. 781–795, 2002.

[28] S. E. Webster, R. M. Eustice, H. Singh, and L. L. Whitcomb, "Preliminary deep water results in single-beacon one-way-travel-time acoustic navigation for underwater vehicles," in *2009 IEEE/RSJ International Conference on Intelligent Robots and Systems*. IEEE, 2009, pp. 2053–2060.

[29] G. Hao, "A 2-legged XY parallel flexure motion stage with minimised parasitic rotation," *Proceedings of the Institution of Mechanical Engineers, Part C: Journal of Mechanical Engineering Science*, vol. 228, no. 17, pp. 3156–3169, 2014.

[30] S. Awtar and A. H. Slocum, "Constraint-based design of parallel kinematic XY flexure mechanisms," *Journal of Mechanical Design*, vol. 129, no. 8, pp. 816–830, 2007.